

Corrosion Behavior of High Strength C71500 Cu-Ni Alloy Pipe in Simulated High Sulfide Polluted Seawater at Different Temperatures

Xin Gao^{1,2}, Hui-bin Wu^{1,*}, Ming Liu^{3,*}, Yuan-xiang Zhang⁴, Feng Gao⁵

¹ Institute of Engineering Technology, University of Science and Technology Beijing, Beijing 100083, China

² General Research Institute of Nonferrous Metals, Beijing 100088, China

³ State Key Laboratory for Strength and Vibration of Mechanical Structures, Xi'an Jiaotong University, Xi'an 710049, China

⁴ The State Key Lab of Rolling and Automation, Northeastern University, Shenyang 110819, China

⁵ School of Materials Science And Engineering, Harbin Institute of Technology, Harbin, 150001, China

*E-mail: whbustb@163.com, liuming0313@xjtu.edu.cn

Received: 4 September 2020 / Accepted: 11 October 2020 / Published: 31 December 2020

By studying the corrosion behavior of high strength C71500 Cu-Ni alloy pipe at the inlet and outlet of heat exchanger in simulated high polluted seawater at different temperatures, which could provide theoretical basis for improving the service life of the alloy. The corrosion mechanism of the alloy was determined by electrochemical techniques such as potentiodynamic polarization curve, electrochemical impedance spectroscopy (EIS) as well as cyclic voltammetry curve (CV) and the morphology and composition of corrosion products were analyzed by immersion test, SEM, EDS, XPS and XRD. The results show that the alloy exhibits activation polarization at all test conditions, the higher the solution temperature, the greater the corrosion rate. When the temperature reaches 35°C, the average corrosion rate of the alloy is stable at about 0.0121 mm/a. In the initial stage of corrosion, diffusion process could be observed. Corrosion products have a certain protective effect, the diffusion process disappears and the EIS shows only capacitive reactance arc with the prolong the immersion time. The addition of high concentration of Na₂S promotes the formation of Cu₂S and the redox process, thus accelerating the corrosion process. At relatively low temperature, the dominant process is Ni dissolution, while the content of Cu and S dissolving increase at high temperature. The thickness and compactness of corrosion products increase with the increasing temperature, which promotes to reach a relative stable corrosion rate. More sulfide species corrosion product could be detected at the low temperature, and the dissolution of copper is the main corrosion process at high temperature.

Keywords: C71500 Cu-Ni pipe; sulfide polluted; temperature; corrosion behavior; seawater

1. INTRODUCTION

High strength C71500 Cu-Ni alloy is widely used in the complex cold and heat interaction environment, such as thermal desalination evaporator, seawater recharge generator, marine ship main power system condenser and heat exchanger, ship power auxiliary heat exchanger and so on [1]. The biological and bacterial reproduction process (algae, marine organisms or microorganisms, sulfide reducing bacteria) promotes the increasing sulfide concentration around the used materials rapidly in marine environment [2]. The existence of sulfide ions and other sulfur-containing substances will accelerate the corrosion process of metal materials [3-6].

The corrosion behavior of Cu in anoxic artificial groundwater in the presence of sulfate reducing bacteria was studied by Huttunen-Saarivirta [7], the addition of microorganisms would change the local surface conditions and the chemical composition of groundwater, thus changing the corrosion mechanism and accelerating corrosion rate. Hazra [8] studied the failure mechanism of Ni-Al bronze impeller in highly polluted seawater and found that the main reason was pitting corrosion along different phase interfaces. Al-Kharafi [9] studied the effect of sulfide ions on long electrochemical film of 90Cu-10Ni alloy in sulfuric acid, sodium sulfate and chloride containing electrolyte at different polarization times. It was found that in the presence of sulfide, Ni has the highest solubility, forming Cu_2S , and then further dissolved the protective alloy film. With the increase of membrane solubility and metal concentration, the polarization resistance of the alloy decreased significantly. X-ray photoelectron spectroscopy (XPS) was applied to deeply analyze the chemical composition of Cu-Ni (90/10) alloy corrosion product in seawater and sulfide polluted seawater with or without inhibitors by Rao [10], the percentage of Cu_2O was found to be much less than that found in the absence of inhibitor. Kong [11] systematically studied the effect of temperature on the corrosion behavior of Cu in simulated high-level radioactive waste environment and found the corrosion resistance of the passive film does not decrease blindly with the increase of temperature, but increases after a certain temperature due to the denser outer layer, and the degree of pitting corrosion decreases with the increase of temperature. Zhang [12] studied Cu-Ni alloy coating and found that the passive film become unstable and the corrosion rate could be greatly increased with the increasing of temperature.

Most of the researches focus on the comparison of the corrosion properties of copper alloys at room temperature [13,14], while the study on the influence of temperature changes on the corrosion behavior of Cu-Ni alloys in the polluted marine environment is relatively less. Meanwhile, the pollution of offshore seawater continues to be intensified with the industrialization, and local sulfur ions exceed the standard seriously. C71500 alloy pipe is widely used as the heat exchanger in various seawater environment. The working temperature of the alloy is changeable and the seawater temperature is different from area to area. In order to improve the service life of C71500 alloy, the corrosion behavior of this alloy in simulated high sulfur content seawater at different temperatures was studied to provide theoretical basis for improving the corrosion resistance.

2. MATERIALS AND METHODS

2.1 Samples and solutions

In this study, high strength C71500 alloy was used. The chemical composition (wt.%) is Ni = 30.54, Mn = 0.93, Fe = 0.80, and the residual is Cu. The microstructure of the material is single-phase [15], and the yield strength after annealing is more than 430 MPa.

The immersion sample was average divided into four parts along the radial direction of the pipe, with a length of 35 mm and a drilling diameter of 2 mm. The 10 × 10 mm specimen was cut along the wall thickness direction of the pipe as the electrochemical testing sample. The outer surface of the pipe was used as the test surface and sealed with epoxy resin. The test surface was grinded to 1500 # with silicon carbide sandpaper, and then placed in a drying dish after the oil was extracted from acetone.

The corrosion solution is composed of 3.5% NaCl + 0.5% Na₂S (wt%). The pH value of the solution is about 8.20, and the temperature is controlled by an electric heating constant temperature water bath at 20, 25, 30, 35, 40 and 45 °C respectively.

2.2 Immersion test

The immersion test was carried out based on the ASTM G31-2012a standard. The immersion time was 24 h. Five parallel samples were selected in each group, three samples were used to measure the average corrosion rate, and the remaining two were used for XPS and XRD analysis. After the test, chemical cleaning method (hydrochloric acid solution with a volume ratio of 2:1) was used to remove the corrosion products on the surface of the weight-loss samples. The samples before and after corrosion were weighed with an electronic balance with a resolution of 0.0001 g. The corrosion rate was calculated by Eq. (1)

$$v = \frac{8.76(m_0 - m_1)}{S_0 t d} \quad (1)$$

where: v is the corrosion rate, mm/a; m_0 is the mass of the sample before corrosion, g; m_1 is the mass of the sample after removing corrosion products, g; S_0 is the area of the tested surface, m²; t is the corrosion test cycle, h; and d is the density of the alloy, g/cm³.

2.3. Electrochemical measurement

The electrochemical measurement was carried out on a CS2350H/CORRTEST electrochemical workstation. The traditional three electrode system was used for the electrochemical test, the outside arc sample was used as the working electrode, the reference electrode was the saturated calomel electrode (SCE), and the auxiliary electrode was the platinum electrode. The open circuit potential (OCP) was measured for 30 min before other electrochemical test was carried out.

The frequency range of electrochemical impedance spectrum (EIS) was 100 kHz-0.01 Hz, and the amplitude of AC excitation signal was 10 mV. The scan rate of potentiodynamic polarization curve was 1 mV/s, and the scan range was from cathodic -0.3 V to anodic 0.8 V (vs. OCP).

The cyclic voltammetry (CV) curve was scanned from cathode to anode, the potential range was - 1.2V~ 0.8V (vs. SCE), the data acquisition frequency was 100 Hz, the scanning rate was 50 mV/s, and the number of cycles was 5.

2.4. Surface analysis

The scanning electron microscope (SEM) of Zeiss brand Gemini 300 was used for microcosmic observation, and the matching EDS was used to analyze the corrosion products chemical composition.

The Rigaku SmartLab 9kW X-ray diffractometer was used to analyze the corroded samples. The measurement range was 20°-100° with a step length of 0.02° and the test results were analyzed by Jade 6.5 software.

A Thermo Fisher Scientific Escalab 250Xi XPS diffractometer was used to analyze the corrosion products. The monochromatic Al-K α X (binding energy 1486.6 eV) ray source was used. The scanning range of the energy spectrum was 0-1200 eV, the scanning interval was 1 eV. The scanning pitch was 0.1 eV, and the spot diameter was 400 μ m. Advantage software was used for peak fitting and analysis, and the C1s spectral line (284.8 eV) was used as the binding energy calibration standard.

3. RESULTS AND DISCUSSION

3.1. Weight loss

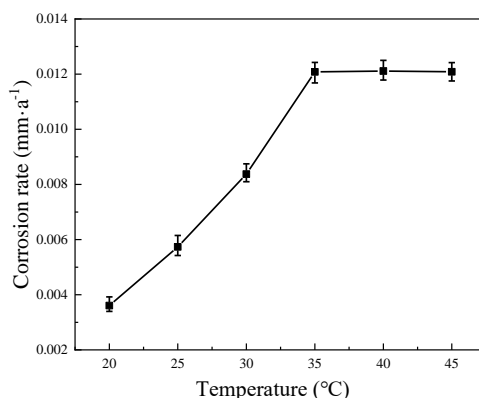


Figure 1. Variation trend of average corrosion rate of C71500 alloy after immersion in 3.5 wt.% NaCl + 0.5wt.% Na₂S solution for 24 h at different temperatures (20, 25, 30, 35, 40 and 45°C).

Fig. 1 shows the variation of average corrosion rate of C71500 alloy samples after immersion in simulated high sulfide polluted seawater at different temperature for 24 h. It can be seen that the minimum corrosion rate is 0.0036 mm/a at 20°C. With gradual increase the temperature, the corrosion rate of alloy gradually increases. When the temperature reaches 35°C, the corrosion rate tends to be

stable in the range of 0.0121 mm/a. The high temperature increases the reaction rate of the alloy thus increasing the corrosion rate at a certain level, the increase of temperature also reduces the dissolved oxygen content in the solution, so the corrosion rate is stable when the temperature exceeds 35°C.

3.2 Electrochemical testing

3.2.1 Polarization curve

Fig. 2 shows the polarization curves of the alloy after immersion in simulated high sulfide polluted seawater environment at different temperatures for 0.5 and 24 h. From the polarization curve of 0.5h immersion in Fig. 2(a), it can be seen that with the increase of temperature, the self-corrosion potential of the alloy moves to negative direction, indicating the increase of temperature increases the corrosion tendency. There is a secondary anodic polarization peak at approximately -0.7 V_{SCE}, indicating the presence of Na₂S promotes the breakdown of anode oxidation films. At this time, the polarization current density of the anode increases with the increasing of temperature at the same potential. The Tafel extrapolation method was used to fit the polarization curve and the electrochemical parameters are listed in Table 1. It can be seen that the self-corrosion current density increases with the increasing of temperature. As shown in Fig. 2(b), some protective corrosion products may be formed that the corrosion potential and anode current density show little difference after immersion for 24 h. The electrochemical parameters fitted by Tafel extrapolation method are listed in Table 2. It can be seen that the corrosion current density changes obviously when the temperature is below 35°C. After reaching 35°C, the self-corrosion current density tends to be stable, which is consistent with the results of corrosion weight loss. These results show that the corrosion rate of C71500 alloy can be greatly influenced when the temperature is below 35°C, and tends to be stable when the temperature exceeds 35°C.

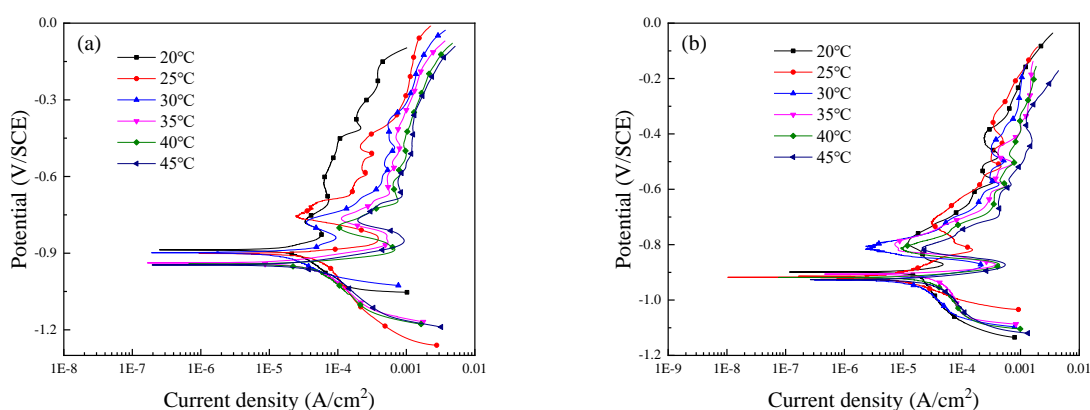


Figure 2. Polarization curves of C71500 alloy immersion in 3.5 wt.% NaCl + 0.5wt.% Na₂S solution at different temperatures (20, 25, 30, 35, 40 and 45°C): (a) 0.5h; (b) 24 h.

Table 1. Fitting parameters of C71500 alloy polarization curves at different corrosion temperatures (20, 25, 30, 35, 40 and 45 °C) after immersion in 3.5 wt.% NaCl + 0.5wt.% Na₂S solution for 0.5 h.

Temperature (°C)	β_a (mV/dec)	β_c (mV/dec)	I_{corr} ($\mu\text{A}/\text{cm}^2$)	E_{corr} (mV)
20	127	-76	27.4	-887
25	30	-60	28.2	-901
30	126	-24	28.4	-922
35	63	-83	29.7	-938
40	30	-101	30.8	-943
45	52	-88	32.0	-946

Table 2. Fitting parameters of C71500 alloy polarization curves at different corrosion temperatures (20, 25, 30, 35, 40 and 45 °C) after immersion in 3.5 wt.% NaCl + 0.5wt.% Na₂S solution for 24 h.

Temperature (°C)	β_a (mV/dec)	β_c (mV/dec)	I_{corr} ($\mu\text{A}/\text{cm}^2$)	E_{corr} (mV)
20	13	-17	2.72	-899
25	22	-25	9.14	-918
30	31	-113	12.2	-928
35	18	-79	18.0	-906
40	24	-86	18.3	-918
45	26	-76	17.6	-926

3.2.2 EIS

The EIS of C71500 alloy immersed in 3.5 wt.% NaCl + 0.5 wt.% Na₂S solution at different temperatures for 0.5 h is shown in Fig. 3. It can be seen from Fig. 3(a) that Nyquist plots are composed of capacitive reactance arc at high frequency and Warburg impedance at medium and low frequency, which indicates that the electrode reaction rate is fast at this time, and diffusion control process is existed; with the increase temperature, the radius of high frequency capacitive reactance arc gradually decreases, indicating that the corrosion rate of alloy increases gradually. From the Bode plots in Fig. 3(b), the impedance modulus $|Z|$ of alloy in the low frequency region gradually decreases with the increase of temperature, indicating the corrosion resistance of the alloy is reduced with the increasing of temperature.

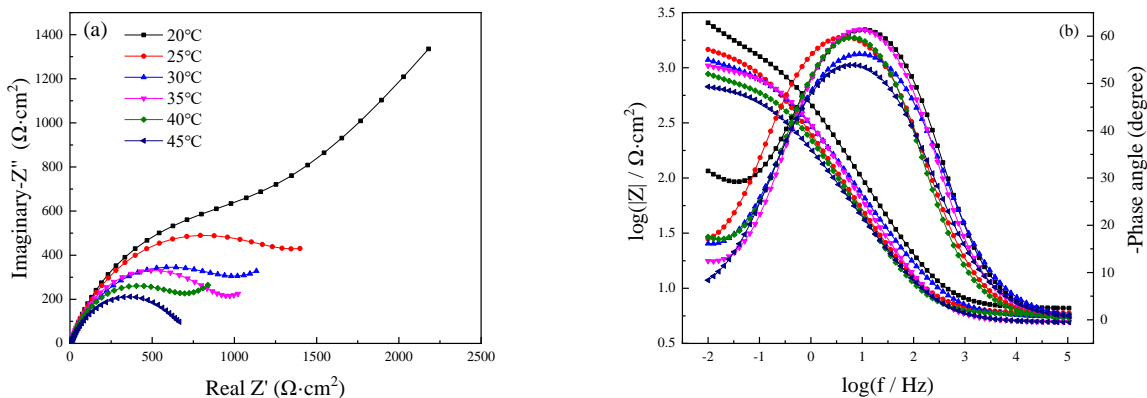


Figure 3. EIS of C71500 alloy immersed in 3.5 wt.% NaCl + 0.5wt.% Na₂S solution at different temperatures (20, 25, 30, 35, 40 and 45°C) for 0.5 h: (a) Nyquist; (b) Bode.

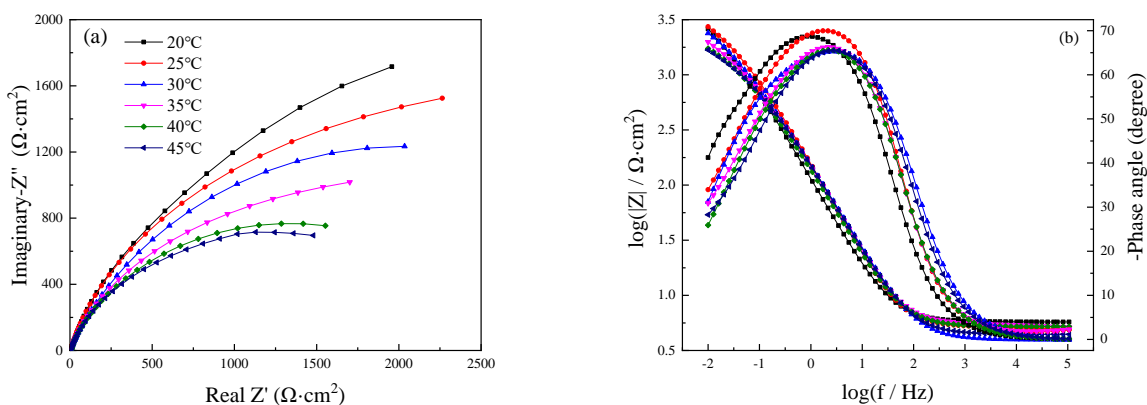


Figure 4. EIS of C71500 alloy immersed in 3.5 wt.% NaCl + 0.5 wt.% Na₂S solution at different temperatures (20, 25, 30, 35, 40 and 45°C) for 24 h: (a) Nyquist; (b) Bode.

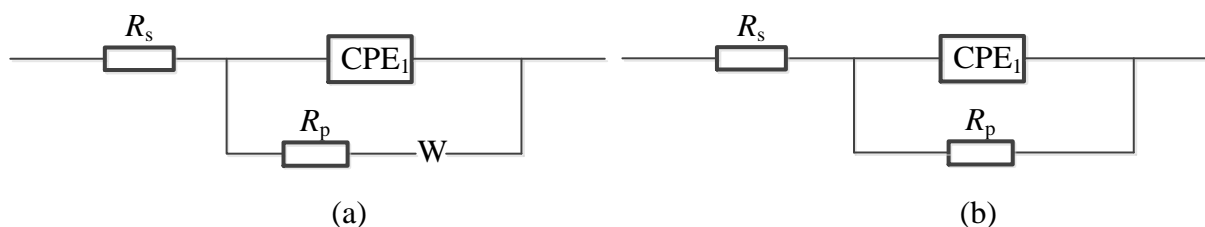


Figure 5. The equivalent circuit of C71500 alloy in 3.5 wt.% NaCl + 0.5 wt.% Na₂S solution at different temperatures (20, 25, 30, 35, 40 and 45°C): (a) 0.5 h; (b) 24 h.

The EIS of C71500 alloy after immersion in 3.5 wt.% NaCl + 0.5 wt.% Na₂S solution for 24 h are shown in Fig. 4. It can be seen from Nyquist plots in Fig. 4(a) that only capacitive reactance arc could be observed, and its radius is significantly larger than that of immersion for 0.5 h, which indicates that some protective corrosion products may be generated, thus hindering the corrosion

process. It can be seen from Bode plots in Fig. 4(b) that $|Z|$ value in the low frequency region decreases with the increase of temperature, which is consistent with Nyquist result.

Base on some research results [16-18], the equivalent circuit shown in Fig. 5 was used to fit the EIS results of alloy after immersion in 3.5 wt.% NaCl + 0.5 wt.% Na₂S solution for different times, where R_s is the solution resistance, R_p is the polarization resistance, CPE_1 is the constant phase element of corrosion product film (Q_{dl}), and W is finite length diffusion Warburg impedance, Z_w . The impedance Z of Q_{dl} can be obtained by [19]:

$$\frac{1}{Z} = Q_{dl}(j\omega)^n \quad (2)$$

where j is the imaginary number ($j^2=1$), ω is the angular frequency ($\omega = 2\pi f$), and n is the exponent of Q_{dl} . When $n = 1$, it can be used as resistance; $n = -1$ can be used as inductance; and $n = 0.5$ is Warburg impedance [20, 21]. In analog equivalent circuit, the CPE is often used instead of pure capacitance element to eliminate dispersion effect caused by electrode surface roughness and other reasons.

The EIS electrochemical parameters fitted by ZsimpWin software at different corrosion temperatures for 0.5 h are shown in Table 3. With the increase of temperature, the charge transfer resistance (R_t) decreases gradually. R_t is 1378 $\Omega \cdot \text{cm}^2$ at 20°C, then decreases to 690 $\Omega \cdot \text{cm}^2$ when the temperature rises to 45°C, with a reduction of 50%. At the same time, the Q_{dl} increases with the increase of temperature, the value of Warburg impedance also increases with the increase of temperature, which further indicates that the increase of temperature accelerates the corrosion rate in the early stage.

Table 3. EIS fitting parameters of C71500 alloy after immersion in 3.5 wt.% NaCl + 0.5 wt.% Na₂S at different temperatures (20, 25, 30, 35, 40 and 45°C) for 0.5 h.

Temperature, °C	R_s , $\Omega \cdot \text{cm}^2$	Q_{dl} ,		R_t , $\Omega \cdot \text{cm}^2$	W $10^{-4} \cdot \Omega^{-1} \cdot \text{cm}^{-2} \cdot \text{s}^{1/2}$
		Y_0 $10^{-6} \cdot \Omega^{-1} \cdot \text{cm}^{-2} \cdot \text{s}^n$	n_1		
20	6.58	429	0.76	1378	22.3
25	5.94	667	0.74	1271	117.0
30	5.47	772	0.70	1032	123.3
35	4.94	942	0.77	920	134.9
40	5.75	978	0.77	695	179.2
45	4.90	1331	0.69	690	1202.0

The EIS electrochemical parameters fitted by the equivalent circuit shown in Fig. 5(b) after 24 h immersion at different corrosion temperatures are shown in Table 4. With the increase temperature, the polarization resistance R_p decreases gradually, which is nearly three times higher than that of immersion for 0.5 h, indicating the corrosion process is obviously inhibited. The largest Q_{dl} is at 20°C, decreases with the increase of temperature, and tends to be stable. The R_p tends to be stable when the temperature exceeds 35°C, which is consistent with weight loss and polarization curve measurement.

Table 4. EIS fitting parameters of C71500 alloy after immersion in 3.5 wt.% NaCl + 0.5 wt.% Na₂S at different temperatures (20, 25, 30, 35, 40 and 45 °C) for 24 h.

Temperature, °C	$R_s,$ $\Omega \cdot \text{cm}^2$	$Q_{dl},$		$R_p,$ $\Omega \cdot \text{cm}^2$
		Y_0 $10^{-6} \cdot \Omega^{-1} \cdot \text{cm}^{-2} \cdot \text{s}^n$	n_1	
20	5.69	2097	0.80	4122
25	5.02	1513	0.81	3419
30	4.88	1674	0.77	3243
35	5.26	1710	0.78	2445
40	5.11	1803	0.78	2029
45	4.35	1659	0.77	1896

3.2.3 CV

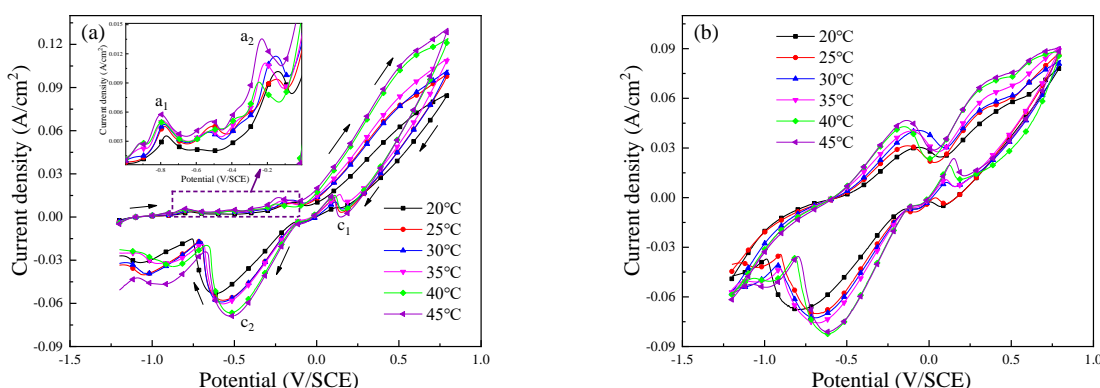
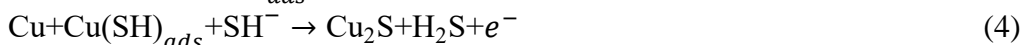
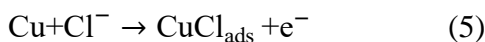


Figure 6. CV curves of C71500 alloy after immersion in 3.5 wt.% NaCl + 0.5 wt.% Na₂S solution at different temperatures (20, 25, 30, 35, 40 and 45 °C): (a) the first cycle; (b) the fifth cycle.

The cyclic voltammetric curves of C71500 alloy in simulated polluted marine environment at different temperatures are shown in Fig. 6. It can be seen from the initial first CV curves in Fig. 6(a), when the electrode potential is less than 0 V_{SCE}, the current density is relatively flat, and no obvious anode current peak could be observed, which may be related to the formation of Cu₂S corrosion product layer [2, 22, 23]. This reaction process is shown in Eqs. (3)- (4).



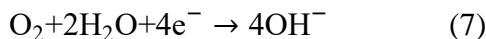
When the anode potential continues to increase, the first obvious anodic oxidation peak a₁ appears at -0.8V_{SCE}, which is mainly because the copper is ionized through the electronic surface under the influence of Cl⁻, thus producing adsorbed CuCl_{ads} on the electrode surface.



Then the formed CuCl_{ads} is easy to dissolve and form the copper complex CuCl₂⁻ [19, 24]:



The cathode reaction rate may be determined by the oxygen reduction kinetics in the neutral solution:



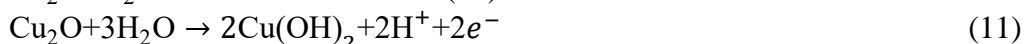
The polarization behavior of C71500 alloy in chloride containing solution is mainly determined by dissolving Cu in soluble CuCl_2^- [25, 26]. Subsequently, in the OH^- containing environment, Cu_2O could be generated through the following reaction:



It is also possible to hydrolyze the resulting soluble ion complexes to form Cu_2O passivelayer [25, 27].



Under oxygen dissolving conditions, the Cu_2O on the outer surface can be converted to Cu^{2+} oxide or hydroxide [28, 29], and the second anode peak (a_2) can be obtained approximately at the potential of $-0.2V_{\text{SCE}}$:



In this process, the oxidation potentials of Cu and Ni are very close, thus only one overlapped oxidation peak could be observed [30]. The two cathode peaks could be detected at about $0.2V_{\text{SCE}}$ and $-0.5V_{\text{SCE}}$, the first peak c_1 could be attributed to the reduction of $\text{Cu}(\text{OH})_2$, the related cathode charge is significantly reduced, and the total current eventually becomes positive. This may be attributed to the loss of CuCl_2^- through transmission to a large amount of solution, which will limit its cathodic reduction in reverse scanning, and the rapid transmission of SH^- will promote the formation of Cu_2S [31]. The peak c_2 is mainly due to the reduction of Cu_2O [28] and the conversion process of Cu_2S and Cu [31].

It can be seen from the peak values in Fig. 6(a) that with the increase of temperature, the current density of anodic peaks gradually increases, indicating that the corrosion process of the alloy can be accelerated by the increase of temperature. At the same time, the cathodic potential shifts to the bottom right and the peak current density also increases with the increasing of temperature. The lower temperature covers a relatively larger potential range, which further indicates the increase of temperature accelerates the dynamic condition of cathodic polarization.

Compared with the first cycle, the anodic peak a_1 in the fifth CV curves (see Fig. 6(b)) disappears and the peak current density of a_2 increases with the increasing of scanning potential, indicating that Cu^{2+} oxide is mainly formed at this time; and with the increase of temperature, the peak current density of oxidation peak further increases and shifts to the right. The peak current density of the reduction peak also increases with the increase of temperature and moves to the left, which indicates that the corrosion process of the alloy is increased.

3.3. Morphology analysis

3.3.1. Macroscopic morphology

Fig. 7 shows the macroscopic morphology of C71500 alloy after immersion in 3.5wt.% NaCl + 0.5wt.% Na_2S solution at different temperatures for 24 h. It can be seen that C71500 alloy mainly exhibits uniform corrosion, and no obvious local corrosion could be detected. At the relatively low

temperature $\leq 35^{\circ}\text{C}$, the surface of the sample were gradually corroded and corrosion products could be observed. With the increase of solution temperature, the amount of corrosion products gradually increased to form different oxidation colors.



Figure 7. Macroscopic corrosion morphology of C71500 alloy after immersion in 3.5 wt.% NaCl + 0.5 wt.% Na₂S solution at different temperatures (20, 25, 30, 35, 40 and 45°C) for 24 h: (a) 20°C; (b) 25°C; (c) 30°C; (d) 35°C; (e) 40°C; (f) 45°C.

3.3.2. SEM analysis

In order to further analyze the corrosion products evolution rule of C71500 alloy with temperature, the microstructure characteristics of the corrosion products after immersion at different temperatures for 24 h were analyzed by SEM. It can be seen from Fig. 8(a) that small granular corrosion products were formed on the surface of the sample at lower temperature (20°C), the product layer is very thin, and the scratch of sandpaper grinding can be clearly observed. When the solution temperature increases to 25°C (Fig. 8(b)), the granular corrosion products gradually increased and could cover the whole surface of the sample, however, the formed corrosion products is relatively loose and could not protect the alloy well. When the temperature continues to increase, the particles in the corrosion products gradually become smaller, the size tends to be stable and gradually compact to cover the whole surface of the sample, so as to effectively isolate the solution from the alloy matrix, thus forming an effective protection barrier to stabilize the corrosion rate.

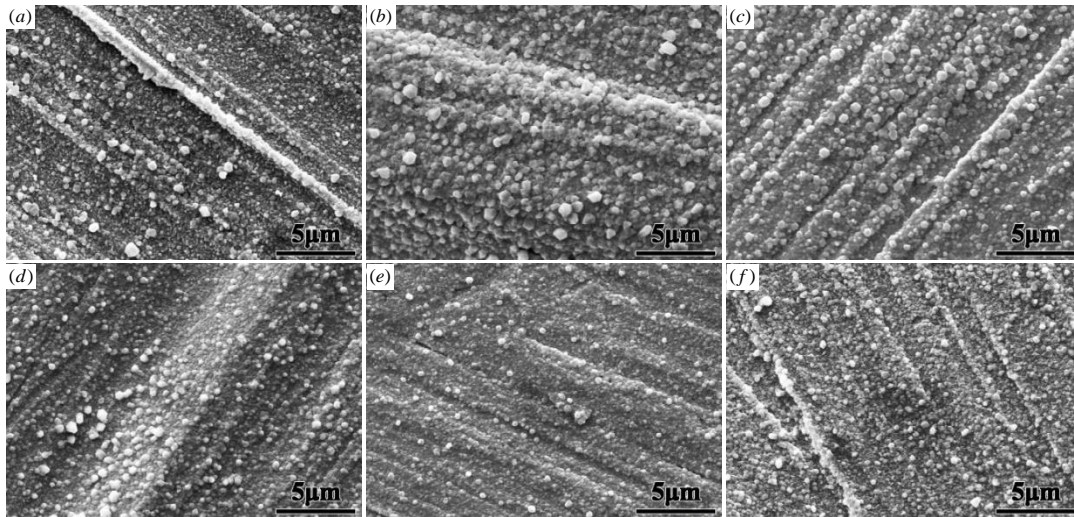


Figure 8. SEM morphology of C71500 alloy after immersed in 3.5wt.% NaCl + 0.5wt.% Na₂S solution at different temperatures for 24 h: (a) 20°C; (b) 25°C; (c) 30°C; (d) 35°C; (e) 40°C; (f) 45°C.

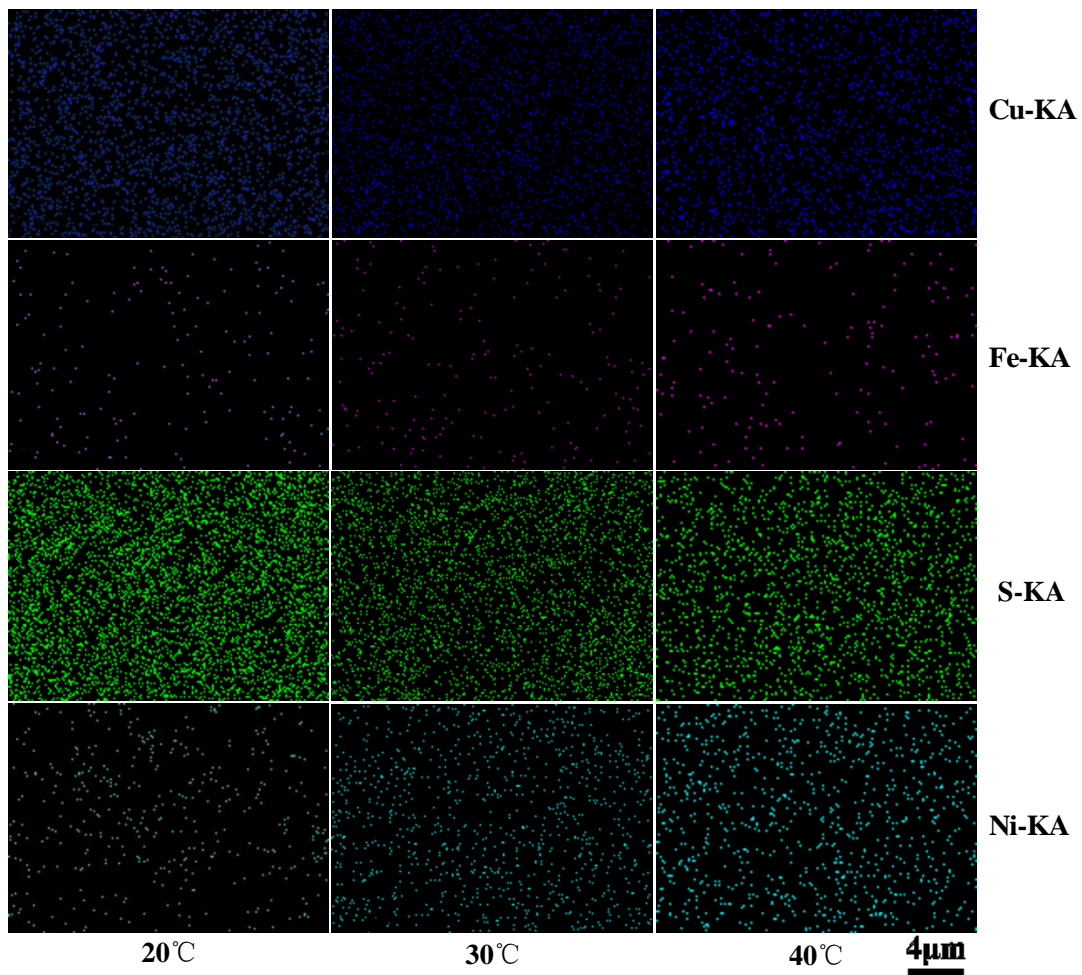


Figure 9. Corrosion products energy spectrum of C71500 alloy after immersion in 3.5wt.% NaCl + 0.5wt.% Na₂S solution at different temperatures (20, 25, 30, 35, 40 and 45°C) for 24 h.

Table 5. Corrosion products EDS analysis results of C71500 alloy after immersion in 3.5wt.% NaCl + 0.5% Na₂S solution at different temperatures (20, 25, 30, 35, 40 and 45 °C) for 24 h (wt.%).

T/ °C	O	S	Mn	Fe	Ni	Cu
20	0.78	17.94	0.27	0.25	6.35	74.41
25	1.46	16.41	0.93	0.53	13.89	66.79
30	0.45	13.74	1.82	0.78	18.67	64.53
35	0.94	10.42	0.41	0.55	24.40	63.27
40	0.23	9.27	0.68	0.81	25.86	63.15
45	0.41	6.38	0.96	0.35	31.37	60.54

The EDS analysis results of C71500 Cu-Ni alloy corrosion products at different temperatures are shown in Table 5. At 20 °C, the content of Ni is significantly lower than that of the basic alloy, which indicates the corrosion process is mainly subjected to nickel dissolving and the results are consistent with some previous conclusions [32]. It can be seen from Fig. 9 and Table 5 that Cu content gradually decreases and Ni content increases gradually, which indicates that the increase of temperature promotes the anodic dissolution of Cu, while the main corrosion process is nickel dissolving at lower temperature, and the change trend of S content is consistent with that of Cu, indicating S participates in the dissolution reaction of Cu.

3.4 XRD analysis

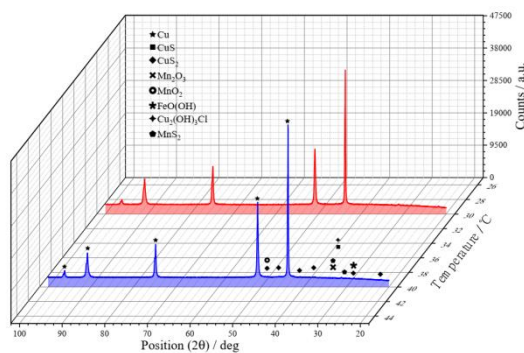


Figure 10. XRD of the C71500 alloy corrosion product after immersion in 3.5 wt.% NaCl + 0.5wt.% Na₂S solution at 30 °C and 40 °C for 24 h.

Fig. 10 shows the XRD comparison diagram of C71500 alloy corrosion product after immersed in 3.5 wt.% NaCl + 0.5 wt.% Na₂S solution at different temperatures for 24 h. It can be observed that the corrosion products are mainly composed of CuS, Cu₂S, Cu₂(OH)₃Cl, Mn₂O, Mn₂O₃, MnS₂, FeO(OH), etc. However, because the immersion time is relatively short, the peaks of the corrosion products are not obvious.

3.5 XPS analysis

The corrosion products on the surface of the samples immersion at 30 and 40 °C for 24 h were also analyzed by XPS. The XPS broad spectrum is shown in Fig. 11. The corrosion products are mainly composed of S, Cu, Cl, O, Mn, Na and other elements. The peak values of Fe and Ni immersed at 30 °C are obvious than that of immersed at 40 °C.

It can be seen from Fig. 12(a) that the Cu 2p of the alloy corrosion product is mainly composed of Cu 2p_{1/2} peak (952 eV) and Cu 2p_{3/2} (932.2 eV). There are polarization and satellite peaks of Cu 2p spectrum line in the 30 °C immersed product film, the S polarization peak is smaller and the polarization peak is more obvious, which indicates that the corrosion products are mainly composed of Cu⁺ and a small amount of Cu²⁺. When the immersion temperature increases to 40 °C, the S polarization peak in the Cu 2p line increases and the satellite peak decreases. In order to further verify the valence state of Cu, the auger spectrum of Cu is analyzed, as shown in Fig. 12(b). It can be seen that the binding energy of auger spectrum of Cu is between 916.5 and 916.8 eV, indicating that the corrosion products are mainly composed of Cu⁺ [33, 34].

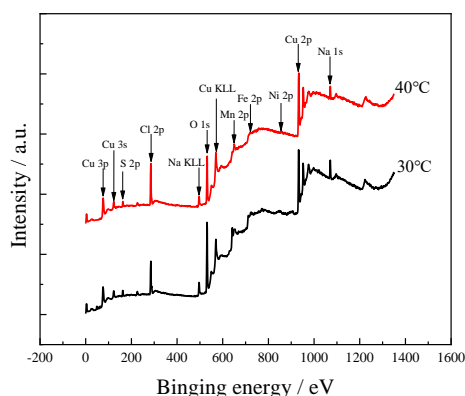


Figure 11. XPS spectra of C71500 alloy corrosion product after immersion in 3.5 wt.% NaCl + 0.5 wt.% Na₂S solution at 30 °C and 40 °C for 24 h.

3.5.1 Cu spectrum

Fig. 13 shows the Cu 2p_{3/2} spectra of corrosion products after immersion at different temperatures. The binding spectra of Cu 2p_{3/2} at high resolution were analyzed in the range of 929-939 eV. It can be seen from Fig. 13(a) that the corrosion products at 30 °C are mainly Cu₂S, Cu₂O and CuCl₂. At this time, Cu₂S is the main corrosion product, which could also be found in the corrosion process of CuZn Alloy in polluted seawater [35], but there is also a certain amount of Cu₂O. The Cu₂O film is a uniform, dense and adherent corrosion product, which can promote the passivation ability of Cu-Ni alloy and improve the corrosion resistance [24]. The corrosion product of Cu²⁺ is mainly CuCl₂. When the temperature rises to 40 °C, the Cu₂O in the corrosion products disappears and the content of CuS increases gradually. Therefore, the corrosion rate of the alloy at 30 °C is much lower than that of at 40 °C.

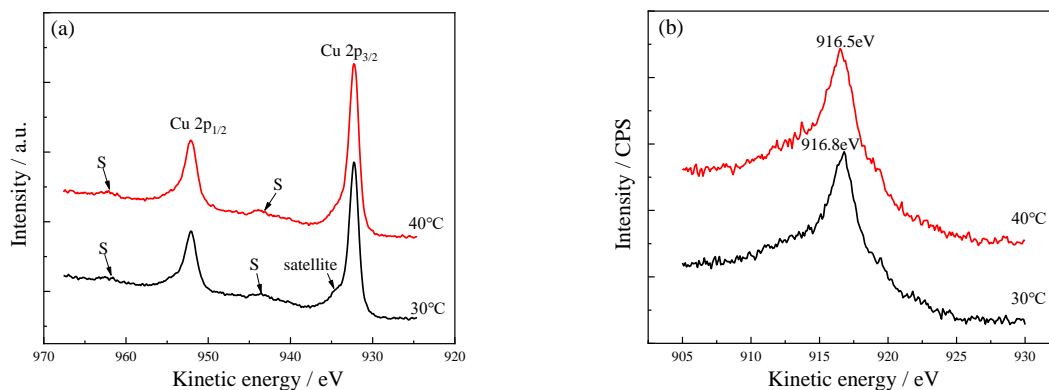


Figure 12. Cu spectrum of C71500 alloy corrosion product after immersion in 3.5 wt.% NaCl + 0.5 wt.% Na₂S solution at 30°C and 40°C for 24 h. (a) Cu 2p; (b) Cu CLM.

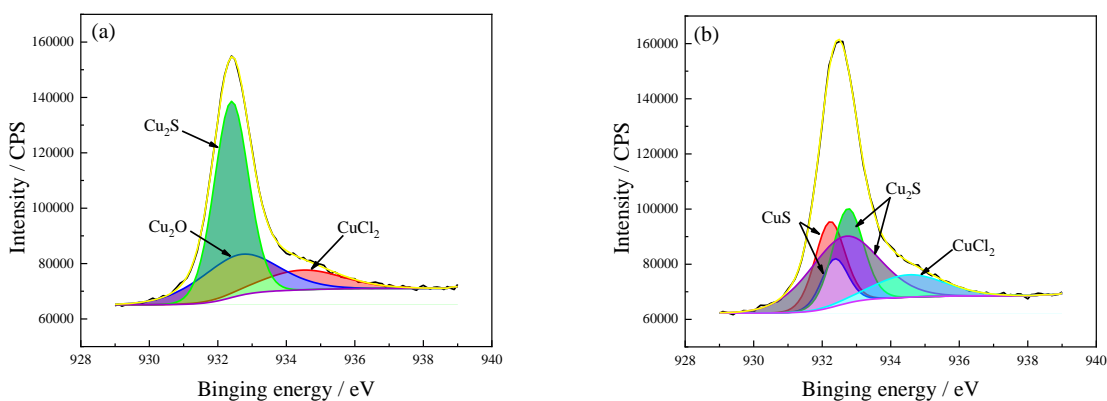


Figure 13. Cu 2p_{3/2} spectra of C71500 alloy corrosion product after immersion in 3.5 wt.% NaCl + 0.5 wt.% Na₂S solution at 30°C and 40°C for 24 h. (a) 30°C; (b) 40°C.

Table 6. The corrosion product phase analysis of Cu 2p_{3/2} spectrum of C71500 alloy after immersion in 3.5 wt.% NaCl + 0.5 wt.% Na₂S solution at 30°C and 40°C for 24 h.

Valence	T(°C)	Proposed compounds	Binding energy(eV)	Intensity area	Atomic(%)
Cu 2p _{3/2}	30	CuCl ₂	934.47	21282.75	13.76
		Cu ₂ O	932.60	43237.89	27.91
		Cu ₂ S	932.40	90373.70	58.33
		CuS	932.22	34584.69	19.66
	40	CuS	932.36	17027.84	9.68
		Cu ₂ S	932.75	39405.02	22.41
		Cu ₂ S	932.63	63363.34	36.04
		CuCl ₂	934.54	21432.53	12.21

3.4.2 Mn spectrum

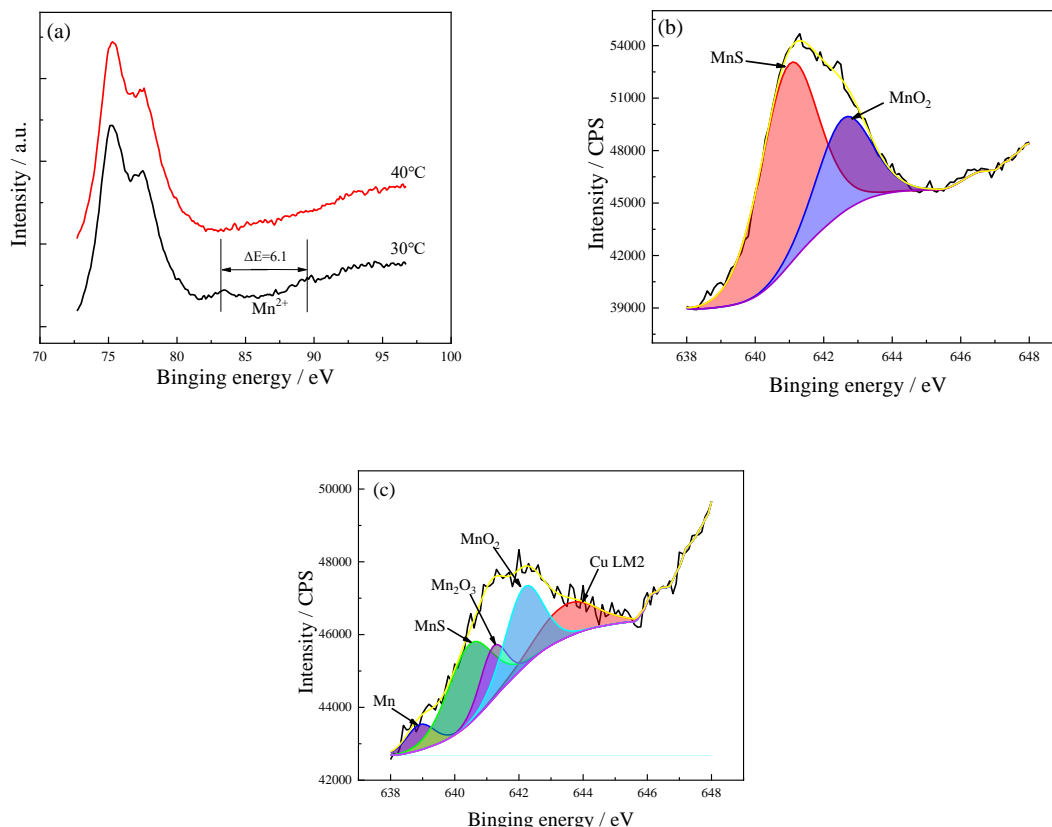


Figure 14. Mn spectrum of C71500 alloy corrosion products after immersion in 3.5 wt.% NaCl + 0.5 wt.% Na₂S solution at 30 °C and 40 °C for 24h. (a)Mn 3s; (b)30 °C-Mn 2p_{3/2}; (c) 30 °C-Mn 2p_{3/2}.

Fig. 14 shows the Mn spectrum of corrosion product after immersion at different temperatures for 24 h. Fig. 14(a) shows the binding spectrum of Mn 3s at high resolution in the range of 72.5-97.5 eV. No small satellite peak could be observed in the 40 °C immersed sample, while the energy difference between the two satellite peaks is 6.1eV at 30 °C, indicating that corrosion product is mainly Mn²⁺.

Table 7. Corrosion product phase analysis of Mn 2p spectrum of C71500 alloy after immersion in 3.5 wt.% NaCl + 0.5 wt.% Na₂S solution at 30 °C and 40 °C for 24h.

Valence	T (°C)	Proposed compounds	Binding energy (eV)	Intensity area	Atomic (%)
Mn 2p _{3/2}	30	MnS	640.98	24706.55	69.63
		MnO ₂	642.58	10767.89	30.37
		Cu LM ₂	643.50	2100.81	18.30
	40	Mn	638.93	780.09	6.78
		MnS	640.47	3864.45	33.61
		Mn ₂ O ₃	641.20	1504.44	13.09

MnO ₂	642.16	3243.04	28.23
------------------	--------	---------	-------

The Mn 2p spectral lines after immersion at different temperatures are shown in Figs. 14(b) and (c). It can be seen that the peak value of Mn 2p_{3/2} at 30°C is greater than that of at 40°C, and the spectral line is more smooth and stable, indicating that the content of Mn in corrosion products at 30°C is higher, which is consistent with the previous energy spectrum results. At 30°C, MnS and MnO₂ are the main corrosion products. When the temperature rises to 40°C, the main components of corrosion products are Mn, MnS, Mn₂O₃ and MnO₂. The increase of high valence of Mn content, especially the Mn oxide content, can migrate through the film and release at the interface of corrosion product/solution. Some of them could also be incorporated into the compounds lattice of corrosion product. High valence ions increase the ion resistance and electronic resistance of Cu₂O lattice, thus improving the corrosion resistance [36]. High valence ion would be formed when these elements are contained in the copper alloy, and the corrosion resistance will be further improved.

3.4.3 O spectrum

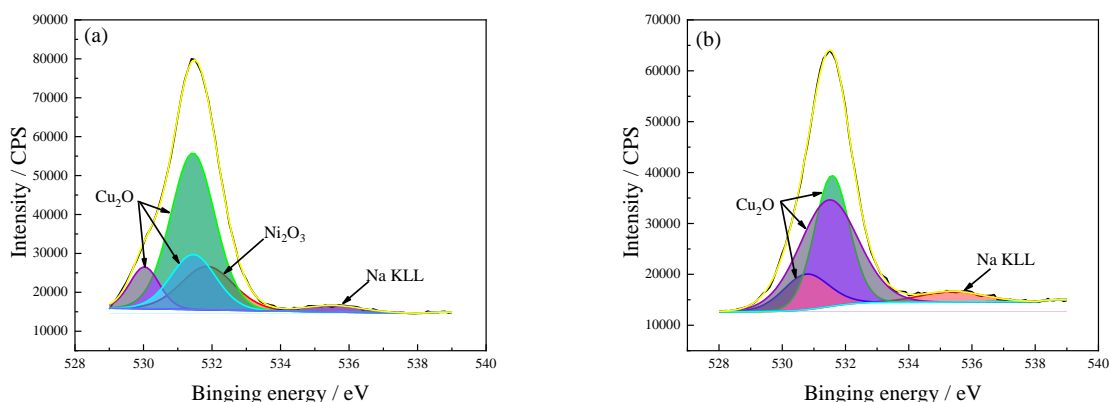


Figure 15. O 1s spectra of C71500 alloy corrosion products after immersion in 3.5 wt.% NaCl + 0.5 wt.% Na₂S solution at 30°C and 40°C for 24 h. (a) 30°C; (b) 40°C.

Table 8. Corrosion product phase analysis of O 1s spectrum of C71500 alloy after immersion in 3.5 wt.% NaCl + 0.5wt.% Na₂S solution at 30°C and 40°C for 24h.

Valence	T (°C)	Proposed compounds	Binding energy (eV)	Intensity area	Atomic (%)
O 1s	30	Ni ₂ O ₃	531.86	21817.24	17.18
		Na KLL	535.55	3466.06	2.73
		Cu ₂ O	531.44	66195.99	52.12
		Cu ₂ O	530.03	11844.93	9.32
	40	Cu ₂ O	531.45	23688.54	18.65
		Na KLL	535.36	5243.58	5.06
		Cu ₂ O	530.76	12791.99	12.31
		Cu ₂ O	531.57	36098.92	34.75

Cu ₂ O	531.47	49740.15	47.88
-------------------	--------	----------	-------

Fig. 15 shows the O 1s spectrum of corrosion product layer after corrosion at different temperatures. It can be seen that the main corrosion products after immersion at 30°C are Cu₂O and Ni₂O₃. With the increase of temperature, Ni₂O₃ could not be detected in the corrosion products. The atom of Ni can be oxidized to form NiO or Ni₂O₃ under the effect of O₂, and then doped into Cu₂O film [37], thus improving the corrosion resistance. Hence, the reason why the corrosion rate is lower at low temperature can be explained.

3.4.4 S spectrum

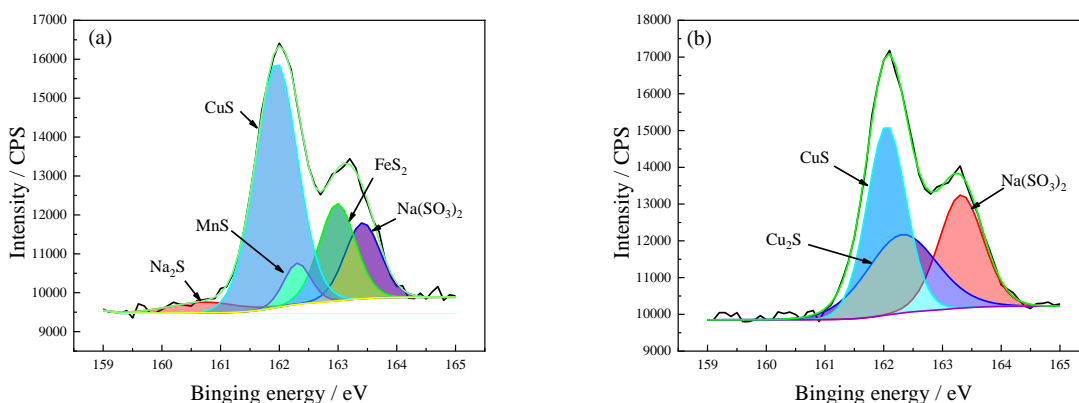


Figure 16. S 2p spectra of C71500 alloy corrosion products after immersion in 3.5 wt.% NaCl + 0.5wt.% Na₂S solution at 30°C and 40°C for 24 h. (a) 30°C; (b) 40°C.

Fig. 16 shows the S 2p spectrum of the corrosion product after immersion at different temperatures. It can be seen that the composition of corrosion products is unstable when immersed at 30°C, and interference peaks of MnS, FeS₂, CuS, Na₂S and Na₂(SO₃)₂ could be observed; when the temperature rises to 40°C, the corrosion products are mainly CuS and Cu₂S, and no sulfide of Fe and Mn could be found, indicating that the dissolution of Cu is the main process at this time, which is consistent with the previous analysis in Fig. 9.

Table 9. Corrosion product phase analysis of S 2p spectrum of C71500 alloy after immersion in 3.5 wt.% NaCl + 0.5 wt.% Na₂S solution at 30°C and 40°C for 24 h.

Valence	T (°C)	Proposed compounds	Binding energy (eV)	Intensity area	Atomic (%)
S 2p	30	Na ₂ S	160.72	409.48	4.00
		Na ₂ (SO ₃) ₂	163.42	1509.41	14.77
		FeS ₂	162.98	1953.98	19.12
		MnS	162.30	619.24	6.06
		CuS	161.95	5730.55	56.05
	40	Na ₂ (SO ₃) ₂	163.31	2969.42	28.12
		Cu ₂ S	162.31	3233.57	30.61

CuS	162.05	4359.27	41.27
-----	--------	---------	-------

4. CONCLUSION

(1) With the increase of temperature, the corrosion rate of C71500 Cu-Ni alloy in 3.5 wt.% NaCl + 0.5 wt.% Na₂S solution increases gradually. When the temperature reaches 35°C, the corrosion rate of the alloy tends to be stable at about 0.0121 mm/a.

(2) The C71500 Cu-Ni alloy shows activated polarization in 3.5% NaCl + 0.5% Na₂S solution, and diffusion could be observed in the initial stage. With the extension of corrosion time, certain protected corrosion products could be formed, the diffusion process disappears, and the impedance spectrum shows only capacitive arc.

(3) The addition of Na₂S is accompanied by the formation of Cu₂S and the oxidation-reduction process, which accelerates the corrosion process of the alloy. The dissolution of Ni is the main process at low temperature, and the decrease of Cu content and the increase of S content at higher temperature.

(4) The thickness of corrosion product increases with the increasing temperature, and the compactness of the corrosion product increases, which makes the corrosion rate of alloy stable at the high temperature.

(5) The content of Cu²⁺ oxides and sulfides in the corrosion products increase with the increasing temperature. The content of sulfide corrosion products species are much more than at low temperature than those in the high temperature. The Cu dissolution is the main corrosion process at high temperature.

ACKNOWLEDGMENTS

The authors gratefully acknowledge the financial supports from the National Natural Science Foundation of China (No. 51801149), the Ministry of Industry and Information Technology of China (TC170A2KN-8) and the International Postdoctoral Exchange Fellowship program 2019 by the Office of China Postdoctoral Council (No. 20190086).

CONFLICTS OF INTEREST

The authors declare no conflict of interest.

References

1. K. Chandra, A. Mahanti, A. P. Singh, V. Kain and H. G. Gujar, *Eng. Fail. Anal.*, 105 (2019) 1328. <https://doi.org/10.1016/j.engfailanal.2019.08.005>
2. M. Guo, J. Chen, T. Martino, M. Biesinger and D. W. Shoesmith, *J. Electrochem. Soc.*, 166 (2019) C505. <https://doi.org/10.1149/2.0611915jes>
3. B. V. Appa Rao and K. Chaitanya Kumar, *Arabian J. Chem.*, 10 (2017) S2245. <https://doi.org/10.1016/j.arabjc.2013.12.026>
4. P. Yi, K. Xiao, C. F. Dong, K. K. Ding, M. Liu and X. G. Li, *Int. J. Electrochem. Sci.*, 10 (2015) 7754. <http://www.electrochemsci.org/papers/vol10/100907754.pdf>
5. Q. N. Song, N. Xu, Y. F. Bao, Y. F. Jiang and Y. X. Qiao, *J. Mater. Eng. Perform.*, 26 (2017) 1.

<https://link.springer.com/article/10.1007/s11665-017-2940-z>

6. M. Liu, S. J. Luo, Y. Shen and X. Z. Lin, *Eng. Fail. Anal.*, 97 (2019) 493.
<https://doi.org/10.1016/j.engfailanal.2019.01.026>
7. E. Huttunen-Saarivirta, P. Rajala and L. Carpen, *Electrochim. Acta*, 203(2016) 350.
<https://doi.org/10.1016/j.electacta.2016.01.098>
8. M. Hazra and K. P. Balan, *Eng. Fail. Anal.*, 70 (2016) 141.
https://www.onacademic.com/detail/journal_1000039507994410_f274.html
9. F. M. Al-Kharafi, A. Abdel Nazeer, R. M. Abdullah and A. Galal, *ECS Trans.*, 64 (2015) 121.
<https://doi.org/10.1149/06426.0121ecst>
10. B. V. A. Rao, K. C. Kumar and N. Y. Hebalkar, *Thin Solid Films*, 556 (2014) 337.
<https://doi.org/10.1016/j.tsf.2013.12.025>
11. D. C. Kong, C. F. Dong, K. Xiao and X. G. Li, *T. of Nonferr. Metal. Soc.*, 27 (2017) 1431.
[https://doi.org/10.1016/S1003-6326\(17\)60165-1](https://doi.org/10.1016/S1003-6326(17)60165-1)
12. Y. Zhang and J. H. Dong, *Foundry Technology*, 32 (2011) 56.
http://en.cnki.com.cn/Article_en/CJFDTOTAL-ZZJS201105014.htm
13. J. Li, C. W. Du, X. G. Li and M. Liu, *Int. J. Electrochem. Sci.*, (2016) 10690.
<https://doi:10.20964/2016.12.46>
14. C. Dehghanian M. Lotfpour and M. Emamy, *J. Mater. Eng. Perform.*, 28 (2019) 2305
<https://doi.org/10.1007/s11665-019-03978-4>
15. X. Gao, H. B. Wu, M. Liu and Y. X. Zhang, *Mater. Charact.*, 169 (2020).
<https://doi.org/10.1016/j.matchar.2020.110603>
16. M. Liu, X. Q. Cheng, X. G. Li, P. Yue and J. Li, *J. Mater. Eng. Perform.*, 25 (2017) 4967.
<https://doi.org/10.1007/s11665-016-2342-7>
17. M. Liu, X. Q. Cheng, X. G. Li, C. Zhou and H. L. Tan, *Constr. Build. Mater.*, Jan.15 (2017) 130.
<https://doi.org/10.1016/j.conbuildmat.2016.10.003>
18. M. Liu, Y. Hao, L. Zheng, L. Niu and D. Miao, *J. Mater. Eng. Perform.*, 28 (2019) 28.
<https://doi.org/10.1007/s11665-019-04469-2>
19. Z. Xiao, Z. Li, A. Zhu, Y. Zhao, J. Chen and Y. Zhu, *Corros. Sci.*, 76 (2013) 42.
<https://doi.org/10.1016/j.corsci.2013.05.026>
20. M. Liu, X. Q. Cheng, X. G. Li and T. J. Lu, *J. Electroanal. Chem.*, 803 (2017) 40.
<https://doi.org/10.1016/j.jelechem.2017.09.016>
21. Nam and N. Dang, *J. Electrochem. Soc.*, 163 (2016) 76.
<https://doi.org/10.1149/2.0281603jes>
22. J. Smith, Z. Qin; F. King, L. Werme, D. W. Shoesmith, *Corrosion*, 63 (2007) 135.
<https://doi.org/10.5006/1.3278338>
23. T. Martino, R. Partovi-Nia, J. Chen, Z. Qin and D. W. Shoesmith, *Electrochim. Acta*, 127 (2014) 439.
<https://doi.org/10.1016/j.electacta.2014.02.050>
24. M. Liu and J. Li, *Materials*, 12(2019) 2164.
<https://doi.org/10.3390/ma12132130>
25. J. P. Ferreira, J. A. Rodrigues and I. T. E. d. Fonseca, *J. Solid State Electrochem.*, 8 (2004) 260.
<https://doi.org/10.1007/s10008-003-0445-1>
26. G. Kear, B. D. Barker, K. Stokes and F. C. Walsh, *J. Appl. Electrochem.*, 34 (2004) 659.
<https://doi.org/10.1023/B:JACH.0000031164.32520.58>
27. E. M. M. Sutter, B. Millet, C. Fiaud and D. Lincot, *J. Electroanal. Chem.*, 386 (1995) 101.
[https://doi.org/10.1016/0022-0728\(95\)03811-T](https://doi.org/10.1016/0022-0728(95)03811-T)
28. M. Saremi and M. Yeganeh, *Mater. Chem. and Phys.*, 123(2010) 456.
<https://doi.org/10.1016/j.matchemphys.2010.04.041>
29. P. L. Bonora, S. Rossi, L. Benedetti and M. Draghetti, *Developments in Marine Corrosion*, (1998) 155.

<https://doi.org/10.1533/9781845698768.155>

30. Mohan and Rajasekaran, *Surf. Eng.*, 27(2011) 519.

<https://doi.org/10.1179/026708410X12786785573472>

31. D. C. Kong, C. F. Dong, A. N. Xu, C. Man, C. He and X. G. Li, *J. Mater. Eng. Perform.*, 26 (2017) 1741.

<https://doi.org/10.1007/s11665-017-2578-x>

32. A. L. Ma, S. L. Jiang, Y. G. Zheng and W. Ke, *Corros. Sci.*, 91 (2015) 245.

<https://doi.org/10.1016/j.corsci.2014.11.028>

33. G. Deroubaix and P. Marcus, *Surf. Interface Anal.*, 18 (2010) 39.

<https://doi.org/10.1002/sia.740180107>

34. A. Galtayries and J. P. Bonnelle, *Surf. Interface Anal.*, 23 (2010) 171.

<https://doi.org/10.1002/sia.740230308>

35. A. P. Patil and R. H. Tupkary, *T. Indian I. Metals*, 61 (2008) 13.

<https://doi.org/10.1007/s12666-008-0060-z>

36. T. Jin, W. Zhang, N. Li, X. Liu and W. Dai, *Materials*, 12 (2019) 1869.

<https://doi.org/10.3390/ma12111869>

37. Q.N. Song, N. Xu, Y.F. Bao, Y.F. Jiang and Y.X. Qiao, *J. Mater. Eng. Perform.*, 26 (2017) 4822.

<https://doi.org/10.1007/s11665-017-2940-z>

© 2021 The Authors. Published by ESG (www.electrochemsci.org). This article is an open access article distributed under the terms and conditions of the Creative Commons Attribution license (<http://creativecommons.org/licenses/by/4.0/>).